Article:
Li, Jianghui, Zakharov, Yuriy orcid.org/0000-0002-2193-4334 and Henson, Benjamin Thomas (2018) Multibranch Autocorrelation Method for Doppler Estimation in Underwater Acoustic Channels. IEEE Journal of Oceanic Engineering. 8093613. pp. 1099-1113. ISSN 0364-9059

https://doi.org/10.1109/JOE.2017.2761478

Multi-branch autocorrelation method for Doppler estimation in UWA channels

Jianghui Li, *Student Member, IEEE,* Yuriy Zakharov, *Senior Member, IEEE,*
and Benjamin Henson, *Student Member, IEEE,*

Abstract

In underwater acoustic (UWA) communications, Doppler estimation is one of the major stages in a receiver. Two Doppler estimation methods are often used: cross-ambiguity function (CAF) method and single-branch autocorrelation (SBA) method. The former results in accurate estimation but with a high complexity, whereas the latter is less complicated but also less accurate. In this paper, we propose and investigate a multi-branch autocorrelation (MBA) Doppler estimation method. The proposed method can be used in communication systems with periodically transmitted pilot signals or repetitive data transmission. For comparison of the Doppler estimation methods, we investigate an OFDM communication system in multiple dynamic scenarios using the *Waymark* simulator, allowing virtual underwater acoustic signal transmission between moving transmitter and receiver. For the comparison, we also use the OFDM signals recorded in a sea trial. The comparison shows that the receiver with the proposed MBA Doppler estimation method outperforms the receiver with the SBA method and its detection performance is close to that of the receiver with the CAF method, but with a significantly lower complexity.

Index Terms

Ambiguity function, autocorrelation, Doppler estimation, OFDM, underwater acoustic communications.

I. Introduction

In underwater acoustic (UWA) communications, due to the slow propagation speed of acoustic waves, the Doppler effect introduces significant distortions in propagated signals [2]–[5]. To achieve a high detection performance, accurate Doppler estimation and compensation techniques are required [2], [6]–[8]. The Doppler effect is caused by transmitter/receiver motion, by surface waves, by fluctuations of the sound speed, and other phenomena [9]–[11]. The Doppler effect on signals is often described as time compression/dilation with a compression factor constant over a measurement interval, i.e., a constant-speed movement [12]–[15]. For specific underwater tasks, such as underwater imaging, environment monitoring, and sea bottom searching, fast-moving platforms such as autonomous underwater vehicles (AUVs) can use complicated trajectories [16]–[21], where the constant-speed assumption is not valid. Such movements require frequent re-estimation of the Doppler effect to support a high detection performance of UWA communications [22]. The Doppler estimation then becomes a complicated task dominating the complexity of the receiver [23].

Many Doppler estimation methods are currently used in UWA communications. One such method involves transmitting Doppler-insensitive preamble and postamble around a data package and estimation of the time difference between their arrivals, transformed into the time-compression factor [2], [24], [25]. This method however assumes that the time compression (the transmitter/receiver velocity) is constant over the data package, which is often not the case with a fast-moving and manoeuvring transmitter/receiver. With fast-varying movements, the Doppler estimation should also be performed within the data package, sometimes requiring updates with every received data symbol [22]. Such Doppler estimation techniques have been specifically developed for different single-carrier modulation schemes [7], [26]–[28]. These techniques however cannot be directly applied to multicarrier transmission, such as the orthogonal frequency-division multiplexing (OFDM); besides, multicarrier schemes are more sensitive to Doppler distortions and require more accurate Doppler estimation [29].

One efficient method of Doppler estimation in multipath channels is based on computing the cross-ambiguity function (CAF) between received and transmitted signals [29]–[31]. The CAF is computed on a two-dimensional (2D) grid of channel delays and Doppler compression factors. The position of maximum of the CAF magnitude over the Doppler grid provides an estimate of the Doppler compression. However, due to a large number of Doppler estimation channels, the CAF method is computationally intensive, even if fast Fourier transforms (FFT) and a two-step (coarse and fine estimation) approach is used to reduce the number of Doppler channels and speed up the computations [8], [12], [23]. Significantly less complicated is the single-branch autocorrelation (SBA) method [12], [32]–[35]. This method is applied to periodic transmitted signals and it exploits the fact that, with a moving transmitter/receiver, the signal period changes; the SBA method measures this change to estimate the time-compression factor. Apart from being of low complexity due to a single estimation branch, another benefit of this method is the efficient combining of multipath components. However, the method can fail in cases where the motion of transmitter/receiver involves accelerations.

Jianghui Li, Yuriy Zakharov and Benjamin Henson are with the Department of Electronic Engineering, University of York, UK, e-mail: jl1384@york.ac.uk, yury.zakharov@york.ac.uk and bth502@york.ac.uk. The material of this paper was partly presented in the UACE-2015 conference in Greece [1].

$$\xrightarrow{x(t)} \boxed{\bar{h}(t,\tau)} \xrightarrow{s_0(t)} \boxed{\delta(\tau-\tau_d(t))} \xrightarrow{s_0(t-\tau_d(t))}$$

Fig. 1. Channel model.

In this paper, we propose a multi-branch autocorrelation (MBA) method that is capable of estimating the Doppler effect in UWA channels with fast moving and manoeuvring transmitter/receiver, having significantly lower complexity than the CAF method and outperforming the SBA method.

One of significant problems of testing signal processing algorithms for UWA communications is the modeling of the signal transmission, taking into consideration the specific time-varying multipath propagation due to the complicated motion of a receiver and transmitter. For such a virtual signal transmission, i.e., the transmission that mimics a real sea trial, the *VirTEX* underwater propagation channel model was developed [36] and used [37]; this model is based on the *Bellhop* ray/beam tracing [38] to compute the channel impulse response in different acoustic propagation environments. A similar approach was implemented in the *Waymark* model [10], [39], [40] developed to efficiently simulate the UWA signal transmission in long communication sessions. We use the Waymark model to test the Doppler estimation methods in communication sessions with complicated motion of the transmitter and receiver.

In this paper, the Doppler estimation methods are implemented in a communication system with guard-free OFDM and superimposed data and pilot signals [10], [30], [31], [41]. The comparison of the three methods (CAF, SBA and MBA) in a number of simulation scenarios, as well as in a real sea trial, shows that the MBA method outperforms the SBA method, also its performance is comparable to that of the CAF method, but with a less complexity.

The paper is organised as follows: Section II describes the transmitted signal, channel model, and receiver. Section III presents the proposed MBA Doppler estimation method. Implementations of the CAF, SBA, and MBA methods are described in Section IV. Sections V and VI compare the Doppler estimators in multiple scenarios, using the Waymark model and data recorded in a sea trial, respectively. Section VII summarizes the paper.

II. TRANSMITTED SIGNAL, CHANNEL MODEL AND RECEIVER

In this section, the transmitted signal, channel model and the receiver structure are described. Transmitted signals that we consider here are guard-free OFDM signals with superimposed pilot signals [23]. However, the proposed Doppler estimation technique can operate with other types of transmitted signals, in which the same signal pattern is repeated in time.

The transmitted signal $x(t)$ consists of a continuous sequence of guard-free OFDM symbols [23], [30]:

$$x_l(t) = \Re\left\{ e^{j2\pi f_c t} \sum_{k=-N_s/2}^{N_s/2-1} [M_p(k) + jD_l(k)] e^{j\frac{2\pi}{T_s}kt} \right\}, \tag{1}$$

where $l = 1, 2, \ldots, L$, L is the number of OFDM symbols in the transmitted data package, $N_s = 1024$ the number of sub-carriers, $f_c = \omega_c/(2\pi) = 3072$ Hz the carrier frequency, $F = 1024$ Hz the frequency bandwidth, $T_s = 1$ s the symbol duration, and $j = \sqrt{-1}$. The sequence $M_p(k) \in [-1, +1]$ is a binary pseudo-random sequence of length N_s, serving as the superimposed pilot signal, the same for all OFDM symbols. Therefore, the pilot signal is periodic in time with the period T_s. The sequence $D_l(k)$ represents the information data in the lth OFDM symbol; it is obtained by interleaving and encoding original data across sub-carriers using rate 1/2 convolutional codes [42].

The UWA channel is often modelled as a time-variant linear system with an impulse response $h(t,\tau)$ that describes multipath and Doppler spreads in the channel. The received signal is then given by

$$r(t) = \int_{-\infty}^{\infty} h(t,\tau)x(t-\tau)d\tau + \nu(t), \tag{2}$$

where $\nu(t)$ is the additive noise. In UWA communications, for a general time-varying multipath channel, different propagation paths, corresponding to different delays τ, might have different Doppler compression factors. The channel can be represented using two time-varying components described by a dominant time-varying channel delay $\tau_d(t)$ and a slower time-varying channel impulse response $\bar{h}(t,\tau)$ as shown in Fig. 1 [23]. The component $\delta(\tau - \tau_d(t))$, where $\delta(\tau)$ is the Dirac delta function, can be thought of as caused by the varying distance between the transmitter and receiver. The component $\bar{h}(t,\tau)$ incorporates differential variations in the lengths of acoustic rays due to the movement. Thus, the time-varying channel impulse response $h(t,\tau)$ can be represented as a convolution of $\delta(\tau - \tau_d(t))$ and $\bar{h}(t,\tau)$. Therefore, the received signal can be represented as $r(t) = s(t) + \nu(t)$, where $s(t) = s_0(t - \tau_d(t))$ and $s_0(t) = \int_{-\infty}^{\infty} \bar{h}(t,\tau)x(t-\tau)d\tau$.

The channel model in Fig. 1 is useful for designing receivers in scenarios with fast moving transmitter and/or receiver. The channel component described by the dominant time-varying delay $\tau_d(t)$ is associated with fastest channel variations, since a small variation in the delay results in a significant variation in the phase of the received signal. However, this component can be described by a few parameters [4], [5]. Therefore, it can be accurately estimated using a Doppler estimator, such as the estimator based on calculation of the ambiguity function [29]–[31] or the autocorrelation [12], [32]–[35], and further equalized using resampling. The other component of the channel representation, described by the impulse response $\bar{h}(t,\tau)$, still contains most of the parameters to be estimated, such as the multipath delays and complex amplitudes. However, these parameters are slower varying in time compared to that of the channel response $h(t,\tau)$. Therefore, an equalizer for the channel component $\bar{h}(t,\tau)$ is easier to build than an equalizer for the channel response $h(t,\tau)$. Many practical receivers are built using this approach, where parameters of the dominant time-varying delay $\tau_d(t)$ are estimated using a Doppler estimator and equalized by resampling the received signal. After that the channel component $\bar{h}(t,\tau)$ is equalized, e.g., using a linear equalizer. For more discussion on this channel representation see [10], [23].

Below, when deriving the proposed MBA Doppler estimator, we will assume that, on the estimation time interval, the impulse response $\bar{h}(t,\tau)$ is time invariant, i.e., $\bar{h}(t,\tau) = \bar{h}(\tau)$, and that the time-varying delay $\tau_d(t)$ is described by a quadratic polynomial, see equation (9). However, when testing this and other Doppler estimators, we will be using more realistic scenarios, with different propagation paths having different Doppler spreads. Note that the scenarios will be defined by the acoustic environment and trajectory of the transmitter/receiver. In the test scenarios, the impulse response $h(t,\tau)$ is incorporated into the data obtained either in a real sea experiment or via virtual signal transmission using the Waymark simulator [10], [39]. Therefore, the channel parameters, including the Doppler parameters associated with the dominant time-varying channel delay $\tau_d(t)$, are not explicitly available for comparison with their estimates. Besides, there are possible multiple variants of splitting $h(t,\tau)$ into the two components $\bar{h}(t,\tau)$ and $\tau_d(t)$. Therefore, we will be assessing the performance of Doppler estimators by comparing the detection performance of a receiver using these estimators.

Fig. 2 shows the block diagram of the receiver. The front-end processing implements the frequency shifting of the received signal $r(t) = s(t) + \nu(t)$ by ω_c, the low-pass filtering, and analog-to-digital conversion of the baseband signal

$$\widetilde{r}(t) = \widetilde{s}(t) + \widetilde{\nu}(t),$$

where $\widetilde{\nu}(t)$ is a baseband noise signal, into signal samples $\widetilde{r}(n)$ taken with a sampling interval $\Delta\tau = T_s/(N_s N_\tau)$, where N_τ is the time oversampling factor, which is set to $N_\tau = 2$ for our experiments.

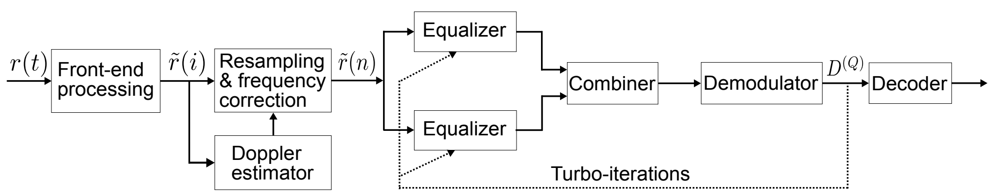

Fig. 2. Block diagram of the receiver for guard-free OFDM signals.

The Doppler estimation consists of two steps: coarse and fine estimation. The coarse estimation is implemented using one of three methods: CAF; SBA; or MBA. The coarse Doppler estimation is performed on a coarse grid of Doppler scaling factors. However, this coarse resolution would not be good enough for equalization and demodulation. Therefore, the coarse estimate is refined by using parabolic interpolation as detailed in [23]. The discrete-time estimates of the Doppler scale factor obtained with the time interval T_{est} (in our experiments, $T_{\text{est}} = T_s/4$) are linearly interpolated, and used to compensate for the dominant time-varying Doppler effect by resampling and frequency correcting the signal $\widetilde{r}(n)$ (see [23] for details).

The resampled and frequency corrected signal $\widetilde{r}(n)$ is divided into two diversity signals, corresponding to odd and even samples of $\widetilde{r}(n)$, respectively. The two signals are independently time-domain equalized. Assuming perfect compensation of the dominant Doppler compression described by the time-varying delay $\tau_d(t)$, the equalization deals with the distortions of the signal caused by the slow variant impulse response $\bar{h}(t,\tau)$ (see Fig. 1). The equalized signals from the two diversity branches are combined and demodulated to produce tentative data estimates, further refined in Q turbo iterations; in our experiments, $Q = 1$. The final data estimate $D^{(Q)}$ is applied to the Viterbi decoder [42] to recover transmitted data.

More details on the operation of the receiver shown in Fig. 2 can be found in [23]. In [23], the CAF Doppler estimator is implemented. It has a high complexity, which is the largest contribution to the total receiver complexity. In this paper, we propose a multi-branch Doppler estimator that has significantly lower complexity and provides almost the same detection performance as the CAF estimator.

III. MULTI-BRANCH AUTOCORRELATION DOPPLER ESTIMATOR

Consider the channel model in Fig. 1. Let the transmitted signal $x(t)$ be represented using an equivalent baseband signal $\widetilde{x}(t)$:

$$\begin{aligned} x(t) &= \Re\{\widetilde{x}(t)e^{j\omega_c t}\} \\ &= \frac{1}{2}\widetilde{x}(t)e^{j\omega_c t} + \frac{1}{2}\widetilde{x}^*(t)e^{-j\omega_c t}, \end{aligned} \quad (3)$$

where $\Re\{\cdot\}$ denotes the real part and $(\cdot)^*$ the complex-conjugate of a complex-valued number. Similarly, we have

$$\begin{aligned} s_0(t) &= \Re\{\widetilde{s}_0(t)e^{j\omega_c t}\} \\ &= \frac{1}{2}\widetilde{s}_0(t)e^{j\omega_c t} + \frac{1}{2}\widetilde{s}_0^*(t)e^{-j\omega_c t}, \end{aligned} \tag{4}$$

where $\widetilde{s}_0(t)$ is an equivalent baseband signal for $s_0(t)$.

Let the signal $\widetilde{x}(t)$ be periodic with a period T_s, so that

$$\widetilde{x}(t+T_s) = \widetilde{x}(t).$$

Assume that the first component in the channel model, shown in Fig. 1, is time invariant, i.e., $\bar{h}(t,\tau) = \bar{h}(\tau)$. Then, the baseband signal $\widetilde{s}_0(t)$ is also periodic with the same period T_s, i.e.,

$$\widetilde{s}_0(t+T_s) = \widetilde{s}_0(t).$$

The second channel component in Fig. 1 is modeled as a time-varying delay $\tau_d(t)$, so the output of the channel without noise is given by

$$\begin{aligned} s(t) &= s_0(t-\tau_d(t)) \\ &= \frac{1}{2}\widetilde{s}_0(t-\tau_d(t))e^{j\omega_c(t-\tau_d(t))} \\ &+ \frac{1}{2}\widetilde{s}_0^*(t-\tau_d(t))e^{-j\omega_c(t-\tau_d(t))}. \end{aligned} \tag{5}$$

In a receiver, typical front-end processing includes a frequency shifting of the received signal $s(t)$ by ω_c via multiplying the signal by $e^{-j\omega_c t}$ and further low-pass filtering. Therefore, the second component in (5) is filtered out, and the front-end processing produces a baseband signal

$$\widetilde{s}(t) = \widetilde{s}_0(t-\tau_d(t))e^{-j\omega_c\tau_d(t)}. \tag{6}$$

A. SBA estimator

The delay $\tau_d(t)$ can often be represented as a linear function of time, described by two parameters, an initial delay a_0 and a time-compression factor a_1 [4], [5]:

$$\tau_d(t) = a_0 + a_1 t, \quad t \in [-\Theta/2, \Theta/2],$$

where Θ is a measurement interval. For estimation of the parameter a_1, the autocorrelation function

$$\rho(\tau) = \int_{-\Theta/2}^{\Theta/2} \widetilde{s}^*(t)\widetilde{s}(t+\tau)dt \tag{7}$$

of the baseband signal $\widetilde{s}(t)$ can then be used [43]. More specifically, a_1 can be estimated by searching for the maximum of $|\rho(\tau)|$ over delays in vicinity of the signal period T_s:

$$\tau_{\max} = \arg \max_{T_s-\tau_M \le \tau \le T_s+\tau_M} |\rho(\tau)|, \tag{8}$$

where $[T_s-\tau_M, T_s+\tau_M]$ is a search interval defined by the maximum possible delay τ_M due to the time compression, i.e., due to the maximum relative velocity between the transmitter and receiver. The ratio $\hat{a}_1 = 1 - T_s/\tau_{\max}$ can be considered as an estimate of a_1 (see below). We call such an estimator of a_1 the SBA estimator.

B. MBA estimator

However, the SBA estimator is limited in accuracy when the Doppler compression factor varies over the measurement interval, i.e., when the delay line in Fig. 1 is described by a polynomial of a higher degree, e.g., if $\tau_d(t)$ is a quadratic polynomial:

$$\tau_d(t) = a_0 + a_1 t + a_2 t^2, \quad t \in [-\Theta/2, \Theta/2], \tag{9}$$

where a_2 is a parameter describing the acceleration. Let a be an acceleration between the transmitter and receiver. Due to this acceleration, the distance $d(t)$ between the transmitter and receiver varies in time as $d(t) = at^2/2$. Since $\tau_d(t) = d(t)/c$, we have $a_2 = a/(2c)$, where c is the sound speed.

In fast-varying channels, for estimation of Doppler parameters, we propose to use the following statistic:

$$\rho(\tau,\Omega,\mu) = \int_{-\Theta/2}^{\Theta/2} \widetilde{s}^*(t)\widetilde{s}(\mu t+\tau)e^{j\Omega t}dt. \tag{10}$$

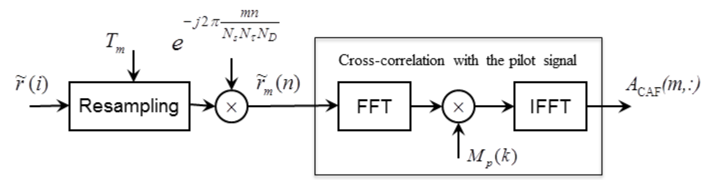

Fig. 3. Computation of one Doppler section of the CAF.

Specifically, the position of the peak of $|\rho(\tau, \Omega, \mu)|$ over delay τ in vicinity of the signal period T_s and over frequency Ω and compression factor μ:

$$\{\tau_{\text{max}}, \Omega_{\text{max}}, \mu_{\text{max}}\} = \arg \max_{\tau,\Omega,\mu} |\rho(\tau, \Omega, \mu)|, \tag{11}$$

will define the Doppler estimate as explained in Appendix A. More specifically, it is shown that the parameter a_1 can be estimated as

$$\hat{a}_1 = 1 - \frac{T_s}{\tau_{\text{max}}} - \alpha \frac{\Omega_{\text{max}}}{2\omega_c}, \tag{12}$$

where $\alpha = [T_s/(k\tau_{\text{max}})]^2 \simeq 1$ and $k = 1 - a_1$. The parameter a_2 can be estimated as

$$\hat{a}_2 = \frac{\Omega_{\text{max}} + a_1(1 - \mu_{\text{max}})\omega_c}{2\mu_{\text{max}}\tau_{\text{max}}\omega_c}, \tag{13}$$

where instead of a_1 its estimate $\hat{a}_1$ can be substituted. Since in many scenarios, $\mu_{\text{max}} \approx 1$, the estimate in (13) can be simplified and made independent of a_1:

$$\hat{a}_2 = \frac{\Omega_{\text{max}}}{2\tau_{\text{max}}\omega_c}. \tag{14}$$

The values μ_{max} and Ω_{max} are inter-dependent as

$$\mu_{\text{max}} = 1 + \frac{\Omega_{\text{max}}}{\omega_c}. \tag{15}$$

This simplifies the Doppler estimation. According to (11), the statistic $|\rho(\tau, \Omega, \mu)|$ needs to be computed at a 3D grid. However, due to the inter-dependence, a 2D grid over (τ, Ω) is sufficient.

If $\Theta F \Omega_{\text{max}}/\omega_c < 1$, we can set $\mu = 1$ in (10), i.e., the resampling is not required, thus further simplifying the signal processing. With high accelerations a and high values of the measurement interval Θ and/or frequency bandwidth F, one of the components in (10) will need to be prescaled with a compression factor μ related to the frequency Ω as $\mu = 1 + \Omega/\omega_c$. In our scenarios, this requirement is satisfied for the whole range of Ω, and therefore we set $\mu = 1$, thus avoiding the resampling.

The estimates of parameters a_1 and a_2, obtained in the MBA Doppler estimator, are used for approximation of the delay $\tau_d(t)$ and resampling the received signal (see Fig. 2).

Note that in the SBA method, the term $\alpha\Omega_{\text{max}}/(2\omega_c)$ as in (12) is ignored, which makes the SBA method less accurate when there is a non-zero acceleration a. However, the main disadvantage of the SBA method compared to the MBA method is that, with non-zero acceleration, the amplitude of the autocorrelation peak in the vicinity of the signal period T_s is reduced. For example, for pseudo-noise signals, such as the m-sequence [42], with a δ-like ambiguity function, the amplitude at $\Omega = 0$ will be close to zero if $\Omega_{\text{max}}\Theta > 2\pi$; e.g., for our scenarios, it corresponds to accelerations $a > 0.5$ m/s^2.

IV. Implementation of Doppler estimators

A. Implementation of CAF method

In the CAF method, $2N_d + 1$ Doppler sections of the ambiguity function are computed with a period T_{est} by cross-correlating the scale-distorted received signal and one period of the pilot signal (see [2] and [23] for more details). The ambiguity function is computed on the *delay-Doppler scale* grid. The delay step on the grid is $\Delta\tau$. The Doppler scale step is chosen so that the corresponding frequency shift Δf is a predefined fraction of the subcarrier spacing F/N_s: $\Delta f = F/(N_s N_D)$, with the frequency oversampling factor N_D set to $N_D = 2$. In [23], it is shown that such a coarse resolution is enough for operation of the receiver, whereas higher N_D would proportionally increase the complexity of the Doppler estimator.

To cover the whole Doppler spread, the cross-ambiguity function $A_{\text{CAF}}(m, n)$, $m = -N_d, \ldots, N_d$, $n = 0, \ldots, N_s N_\tau - 1$, has $2N_d + 1$ Doppler sections. The $\hat{m}$-th Doppler section with the maximum magnitude indicates the coarse Doppler estimate:

$$[\hat{m}, \hat{n}] = \arg \max_{m,n} |A_{\text{CAF}}(m, n)|.$$

One Doppler section $A_{\text{CAF}}(m,:)$ is computed as shown in Fig. 3. The input signal $\tilde{r}(i)$ with the original sampling rate f_s is resampled and frequency shifted according to the mth scale factor $1+d(m)$, where $d(m) = m\Delta f/f_c = mF/(N_s N_D f_c)$ and $m = -N_d, \dots, N_d$. The resampling interval T_m for the mth Doppler section is given by $T_m = 1/[FN_\tau(1+d(m))]$. The resampling is based on the linear interpolation and compensates for the time scale with the factor $1+d(m)$.

Denoting $\hat{r}(t)$ as a continuous-time signal that would be obtained via the linear interpolation of $\tilde{r}(i)$, after the resampling and frequency correction, we have $\tilde{r}_m(n) = \hat{r}(nT_m)\exp(-j2\pi mn/N_s N_\tau N_D)$. Such a Doppler-like distorted received signal is correlated with one period of the pilot signal $p(i)$:

$$A_{\text{CAF}}(m,n) = \sum_{i=0}^{N_\tau N_s - 1} \tilde{r}_m(i) p^*(i \oplus n), \tag{16}$$

where $\oplus$ denotes the cyclic shift over the period $N_s N_\tau$, $(\cdot)^*$ denotes complex conjugate, and

$$p(i) = \sum_{k=-N_s/2}^{N_s/2-1} M_p(k) e^{-j\frac{2\pi}{N_s N_\tau}ki}. \tag{17}$$

This computation can be done using the FFT and IFFT as shown in Fig. 3. The use of the FFT and IFFT for computing the cross-correlation is possible because OFDM symbols have no guard interval, the pilot signal is periodic, and the orthogonality interval is equal to the OFDM symbol duration. The position of the peak of the CAF magnitude indicates the coarse Doppler estimate: $\hat{a}_1 = -d(\hat{m})/[1+d(\hat{m})]$. The FFT in Fig. 3 is of size $N_s N_\tau$; such a time oversampling allows avoiding the interference at boundary subcarriers (close to the frequencies $f_c - F/2$ and $f_c + F/2$). Although the frequency-domain multiplication by the pilot sequence $M_p(k)$, $k = 0, \dots, N_s - 1$, is only over N_s subcarriers, the IFFT in Fig. 3 is also of size $N_s N_\tau$ with zero-padding of the rest $N_s(N_\tau - 1)$ FFT bins; this provides more accurate position estimation for the peak of the ambiguity function.

B. Implementation of SBA method

The SBA method is implemented by computing the autocorrelation of the received signal,

$$A_{\text{SBA}}(\tau) = \sum_{i=0}^{N_\tau N_s - 1} \widetilde{r}^*(i)\widetilde{r}\left(i + \frac{\tau}{\Delta\tau}\right), \tag{18}$$

where $\tau/\Delta\tau \in \{N_\tau N_s - \tau_M/\Delta\tau, N_\tau N_s + \tau_M/\Delta\tau\}$, and finding the maximum

$$\tau_{\text{max}} = \arg\max_{\tau} |A_{\text{SBA}}(\tau)|.$$

The parameter a_1 is then estimated as in (12) with $\Omega_{\text{max}} = 0$.

C. Implementation of MBA method

The MBA method is implemented by computing $2N_d + 1$ autocorrelation functions with a set of frequency shifts Ω_m, $m = -N_d, \dots, N_d$:

$$A_{\text{MBA}}(\tau, \Omega_m) = \sum_{i=0}^{N_\tau N_s - 1} \widetilde{r}^*(i)\widetilde{r}\left(i + \frac{\tau}{\Delta\tau}\right) e^{j\Omega_m \Delta\tau i}, \tag{19}$$

where $\tau/\Delta\tau \in \{N_\tau N_s - \tau_M/\Delta\tau, N_\tau N_s + \tau_M/\Delta\tau\}$ and $\Omega_m = 2\pi\Delta f m$. The parameter a_1 is then estimated as in (12) with $\alpha = 1$ and a_2 is estimated as in (14), where

$$\{\tau_{\text{max}}, \Omega_{\text{max}}\} = \arg\max_{\tau, \Omega_m} |A_{\text{MBA}}(\tau, \Omega_m)|.$$

Note that the complexity of each of the three methods is directly proportional to the number of Doppler estimation sections $(2N_d + 1)$. It is shown in Appendix B that the complexity of computing a single Doppler section is approximately the same in all the methods. Therefore, to compare the complexity, we need to know the number of Doppler sections. The SBA method is the simplest one since it requires a single Doppler section, $N_d = 1$. For the CAF method, N_d is approximately given by

$$N_d = \text{round}\left[\frac{V_{\text{max}} f_c}{c\Delta f}\right], \tag{20}$$

where round$[\cdot]$ denotes the closest integer number, $\Delta f = 0.5$ Hz the Doppler frequency step, $f_c = 3072$ Hz the carrier frequency, $c = 1500$ m/s the underwater sound speed, and V_{max} the maximum speed of transmitter/receiver. The MBA method is an extension of the SBA method as (19) is an extension of (18). Since with (19), the one-dimensional search is replaced

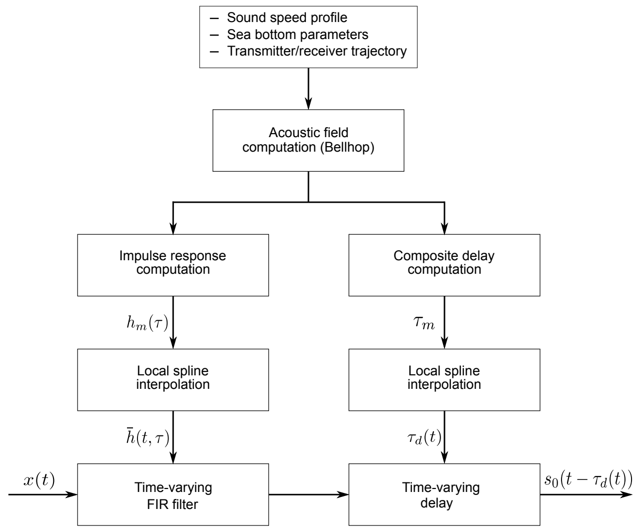

Fig. 4. A block diagram of the Waymark underwater acoustic simulator.

with a two-dimensional search, the complexity of the MBA method is higher than that of the SBA method. For the MBA method, N_d is given by

$$N_d = \text{round}\left[\frac{U_{\max} T_s f_c}{c\Delta f}\right], \tag{21}$$

where $U_{\max}$ is the maximum acceleration of transmitter/receiver. In typical scenarios, $U_{\max} T_s < V_{\max}$, and therefore the number of Doppler sections N_d in the MBA method is typically smaller than N_d in the CAF method, as can be seen from comparison of (20) and (21), thus reducing the complexity of the MBA method.

V. Numerical results

In this section, we investigate the detection performance of three versions of the receiver of guard-free OFDM signals, shown in Fig. 2. These versions differ in the Doppler estimator, which are the CAF, SBA, or MBA estimator. The investigation is performed using the Waymark simulator [10], [39], [40] to model the time-varying multipath distortions of signals, caused by moving transmitter and/or receiver in specific acoustic environments. The required signal-to-noise ratio (SNR), from 7 dB to 17 dB, is then achieved by adding independent Gaussian noise to the distorted signal. The SNR is defined as the ratio of the energy of the distorted signal over the whole length of the communication session to the noise energy over the same time interval, in the frequency bandwidth of the transmitted signal (from 2560 Hz to 3584 Hz).

The Waymark channel simulator [10], [39], [40] shown in Fig. 4 implements the channel model in Fig. 1 using the acoustic field computation for an environment defined by a sound speed profile (SSP) and acoustic bottom parameters. This is done using the Bellhop ray/beam tracing [38]. Using the ray parameters, the Waymark simulator computes the dominant delays $\{\tau_m\}$ and channel impulse responses $\{h_m(\tau)\}$ for a set of points (waymarks) along the transmitter/receiver trajectory. These are spline-interpolated in time to obtain the continuous time-varying delay $\tau_d(t)$ and impulse response $\bar{h}(t,\tau)$; in the simulator, the continuous time t is treated as the discrete time at a sampling rate high enough to accurately represent the communication signal. The (fractional) delay $\tau_d(t)$ is then implemented by interpolation of the signals, whereas the convolution with the impulse response $\bar{h}(t,\tau)$ is implemented using a time-varying finite impulse response (FIR) filter. In this paper, the Waymark simulator is used for numerical investigation of the Doppler estimation methods in a number of scenarios. Note that sea trials with such scenarios would otherwise be difficult to conduct. However, data from a sea trial are also used for investigation of the Doppler estimators, see Section VI.

In the Waymark simulation, the following three scenarios are considered:

- Scenario 1: the transmitter moves with a sinusoid-like trajectory towards the receiver at a speed of 6 m/s, while the receiver is stationary, as shown in Fig. 5(a);
- Scenario 2: the transmitter moves with a sinusoid-like trajectory past the receiver at a speed of 6 m/s, while the receiver moves towards the transmitter at a speed of 6 m/s, as shown in Fig. 5(b);
- Scenario 3: the transmitter performs a slow *flower circle* movement, while the receiver moves towards the transmitter at a speed of 6 m/s, as shown in Fig. 5(c).

The depth of both the transmitter and the receiver is 60 m. The data transmission lasts for 200 s, i.e., $L = 200$ OFDM symbols are transmitted in a communication session.

(a) Transmitter moves towards receiver (Scenario 1).

(b) Transmitter moves past receiver (Scenario 2).

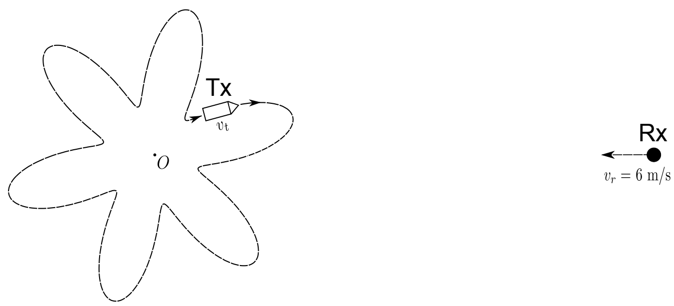

(c) Flower circle movement of the transmitter; O is the center of the flower (Scenario 3).

Fig. 5. Simulation scenarios (top view; Tx is the transmitter, and Rx is the receiver).

A. Scenario 1

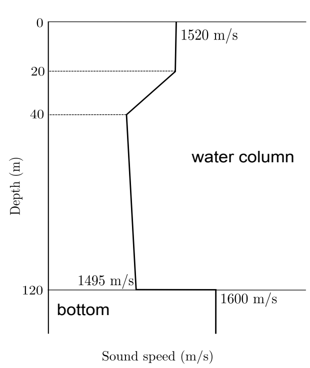

(a) Summer SSP

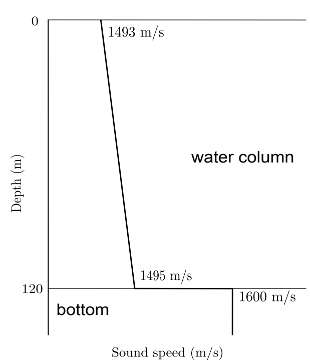

(b) Winter SSP

Fig. 6. The shallow water SSPs [44], [45] used in the simulation.

In this scenario, two shallow water environments are considered, with summer and winter SSPs [44], [45], shown in Fig. 6(a) and Fig. 6(b), respectively. The transmitter moves towards the receiver with a sinusoid-like trajectory as shown in Fig. 5(a). Such a movement can be caused when a transducer is towed by a surface vessel. Indeed, the sinusoid-like trajectory is only an approximation of a real movement affected by the surface waves [10]. The distance $\mathrm{D}(t)$ between the transmitter and receiver varies in time as

$$\mathrm{D}(t) = \mathrm{D}_0 - v_t t + K \sin\left(\frac{2\pi t}{T}\right), \tag{22}$$

where D_0 is an initial distance at $t = 0$, $K = 2$ m is the sinusoid amplitude, $T = 10$ s is a typical period of surface waves, and $v_t = 6$ m/s is the speed of the vessel. Thus, the maximum speed between the transmitter and receiver is $V_{\max} = 7.3$ m/s and the maximum acceleration $U_{\max} = 0.79$ m/s^2.

Based on the maximum velocity and acceleration, from (20) and (21) we obtain the number of Doppler sections in the CAF and MBA estimators as 61 and 7, respectively. As the complexity of the estimators is proportional to the number of Doppler sections, it can be seen that the MBA estimator requires almost 9 times less computations. Indeed, the SBA method requires a single Doppler section and it has the lowest complexity of the three methods. However, as will be seen from our investigation, the SBA method is incapable of providing reliable detection.

1) Experiment with the summer SSP: This experiment starts at the distance $D_0 = 10$ km. Fig. 7(a) shows fluctuations of the channel impulse response. Fig. 8(a) shows the bit-error-rate (BER) performance of the receiver with the three Doppler estimation methods. It can be seen that the SBA method is unable to provide a reliable detection, whereas the MBA estimator provides a BER performance comparable to that of the CAF method.

2) Experiment with the winter SSP: In this case, the SSP is as shown in Fig. 6(b), and the initial distance is set to $\mathrm{D}_0 = 20$ km. Fig. 7(b) shows fluctuations of the channel impulse response in this case. It is seen that the multipath structure of this channel is more complicated than in the channel with the summer SSP. However, as seen in Fig. 8(b), the proposed MBA method still provides a performance comparable to that of the CAF method. It is also seen that the SBA method cannot provide reliable detection.

B. Scenario 2

In this scenario, the summer SSP is used for simulation, and the distance $\mathrm{D}(t)$ between the transmitter and receiver is described as

$$\mathrm{D}(t) = \sqrt{(\mathrm{D}_0 - v_r t)^2 + (v_t t + K \sin(2\pi t/T))^2}, \tag{23}$$

where $\mathrm{D}_0 = 2$ km is the initial distance at $t = 0$, $K = 2$ m, $T = 10$ s and $v_t = v_r = 6$ m/s. Fig. 7(c) shows fluctuations of the channel impulse response in this scenario. Fig. 8(c) shows the BER performance of the receiver with the three Doppler estimation methods. It can be seen that, at SNRs higher than 15 dB, the CAF method provides error-free transmission, while the MBA method allows the error-free transmission at SNRs higher than 13 dB. It can also be seen that the SBA method shows poor performance, whereas the MBA estimator again shows a performance similar to that of the CAF method.

In this scenario, the maximum transmitter/receiver velocity is $V_{\max} = 6$ m/s and the maximum acceleration is $U_{\max} = 0.7$ m/s^2. From (20) and (21) we obtain that the CAF method requires 51 Doppler sections and the MBA method requires 7 Doppler sections, i.e., the MBA method requires about 7 times less computations than the CAF method.

C. Scenario 3

AUVs can use complicated trajectories for underwater imaging, monitoring and sea bottom searching [16]–[21]. A complicated trajectory is considered in this scenario as shown in Fig. 5(c); the trajectory of the transmitter looks like a petaled flower. The receiver moves at a speed of $v_r = 6$ m/s. The distance $\mathrm{D}(t)$ between the transmitter and receiver is described as

$$\begin{aligned} D(t) =& \sqrt{(D_0 - v_r t)^2 + [K \sin(12\pi t/T) + 2]^2} \\ & \overline{-2(D_0 - v_r t)[K \sin(12\pi t/T) + 2] \cos(2\pi t/T)}, \end{aligned} \tag{24}$$

where $D_0 = 5$ km is the initial distance at $t = 0$ between the central point (point O in Fig. 5(c)) of the flower and receiver, $K = 2$ m, and $T = 100$ s the period of passing one flower circle; the external radius of the flower is 3 m.

Fig. 7(d) shows fluctuations of the channel impulse response in this scenario and Fig. 8(d) shows the BER performance of the receiver. It can be seen that the SBA method is outperformed by the other two methods, which show similar performance.

In this scenario, the transmitter moves with a relatively low time-varying velocity, $v_t \leq 0.38$ m/s. The maximum transmitter/receiver velocity is $V_{\max} = 6.8$ m/s, and the maximum acceleration is $U_{\max} = 0.29$ m/s^2. From (20) and (21), we obtain that the CAF method requires 59 Doppler sections and the MBA method requires only 3 Doppler sections; thus the MBA method has almost 20 times less complexity than the CAF method.

From this numerical investigation, we can conclude that the proposed MBA method significantly outperforms the SBA method. In fact, the BER performance achieved with the SBA method does not improve with increased SNR. This is explained by the fact that under a high acceleration, the received signal at delays close to T_s is decorrelated. Fig. 12(b) shows that, without the frequency correction (as in Doppler section 4), the autocorrelation peak is close to zero. However, with the frequency correction (as in Doppler section 2), the high autocorrelation is recovered. Therefore, in channels with high acceleration, the SBA method is not capable of providing a reliable detection, while the MBA method shows a high performance. It can also be seen that the MBA method provides a performance similar to that of the CAF method. However, the complexity of the MBA method is significantly lower than the CAF complexity.

D. MSE performance of the Doppler estimators

Since the ultimate purpose of the Doppler estimators is to achieve a good detection performance, in the previous part of this section we compared the BER performance of a receiver using these estimators. However, when dealing with an estimation problem, it is often desirable to obtain the MSE (Mean-Squared Error) performance of estimators to compare their accuracy. The MSE results can also be used to explain the receiver BER performance. However, in our scenarios defined by the acoustic

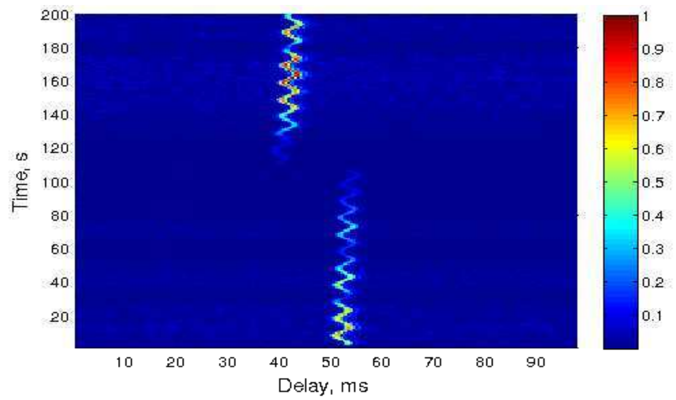

(a) Summer SSP, transmitter moves towards receiver (10 km, Scenario 1).

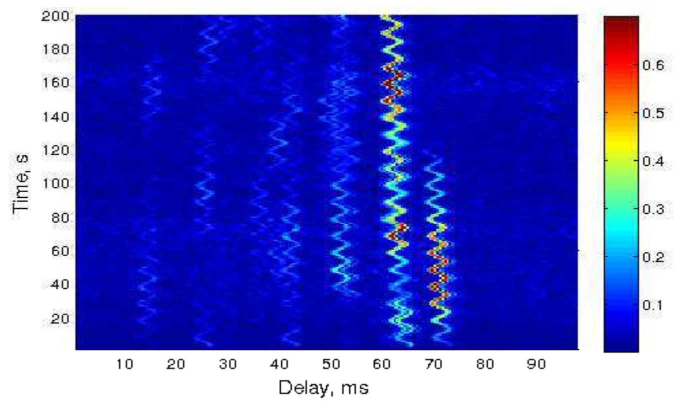

(b) Winter SSP, transmitter moves towards receiver (20 km, Scenario 1).

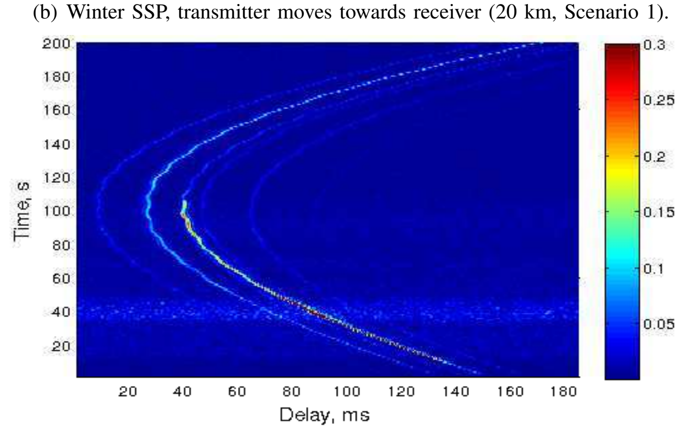

(c) Summer SSP, transmitter moves past receiver (2 km, Scenario 2).

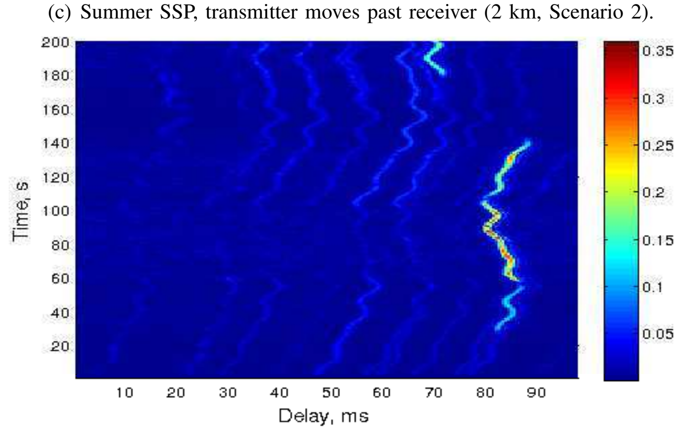

(d) Summer SSP, flower circle movement (5 km, Scenario 3).

Fig. 7. Fluctuations of the channel impulse response in the four simulation scenarios (distance).

environment and trajectory of the transmitter/receiver, it is not directly possible to compute the MSE. The time-varying impulse response $h(t,\tau)$ is incorporated into the received signal obtained via virtual signal transmission in the Waymark simulator. Therefore, the Doppler parameters associated with the dominant time-varying channel delay $\tau_d(t)$ are not explicitly available for comparison with their estimates. Moreover, all these parameters are time-varying, i.e., there is no single Doppler compression factor or the acceleration parameter for comparison.

To overcome this difficulty, we consider scenarios that are somewhat similar to scenarios described above and, at the same time, make the true Doppler parameters available for comparison with their estimates. In these 'synthetic' scenarios, the dominant delay $\tau_d(t)$ is described by the model (9) with parameters a_1 and a_2 randomly generated. More specifically, the velocity v and acceleration a are uniformly distributed in intervals defined by each scenario, and parameters a_1 and a_2 are computed as $a_1 = -v/c$ and $a_2 = a/(2c)$. The impulse response $\bar{h}(t,\tau)$ is time-invariant; it is generated as an FIR impulse response with non-zero taps having relative delays and amplitudes close to those shown in Fig. 7. We run $N_{\text{MC}} = 1000$ simulation trials, with a single measurement of the Doppler compression factor a_1 in each trial, and for every estimator compute the Root MSE (RMSE):

$$\text{RMSE} = \left[\frac{1}{N_{\text{MC}}}\sum_{i=1}^{N_{\text{MC}}}\left(a_1^{(i)} - \hat{a}_1^{(i)}\right)^2\right]^{1/2}, \tag{25}$$

where $a_1^{(i)}$ is the true value of the parameter a_1 in the ith trial and $\hat{a}_1^{(i)}$ is its estimate.

The simulation results are shown in Fig. 9. In the scenario with the transmitter moving towards receiver and summer SSP (see Fig. 9(a)), the velocity v is randomly generated within the interval $[4.7, 7.3]$ m/s and the acceleration a is randomly generated within the interval [-0.79, 0.79] m/s^2; the channel is single-path. It can be seen that, in the SNR range [7, 17] dB (used for the analysis of the BER performance) the CAF and MBA estimators significantly outperform the SBA estimator. This is consistent with the BER performance in Fig. 8(a). With the winter SSP (see Fig. 9(b)), the velocity and acceleration are the same as with the summer SSP, but the channel has 7 multipath components in a delay interval of 55 ms, all with equal powers. Again, the MBA and CAF estimator significantly outperform the SBA estimator, which is consistent with the BER performance in Fig. 8(b). With the transmitter moving past the receiver (see Fig. 9(c)), the velocity v and acceleration a are randomly generated within intervals [-6, 2.2] m/s and [-0.7, 0.7] m/s^2, respectively. In the channel, there are 5 multipath components within a delay interval of 55 ms with relative powers [0.5, 1, 1, 0.5, 0.5]. The MSE performance of the CAF and MBA estimators are significantly better than that of the SBA estimator, which matches to the BER performance in Fig. 8(c). Finally, Fig. 9(d) shows the MSE performance in the scenario with the flower circle movement of the transmitter. The velocity v and acceleration a are randomly generated within intervals [-6.7, -5.3] m/s and [-0.29, 0.29] m/s^2, respectively. In the channel, there are 9 multipath components within a delay interval of 80 ms with relative powers 0.5 with respect to the multipath component with the longest delay. Now, in the SNR interval [7, 17] dB, although the CAF and MBA estimators outperform the SBA estimator, the performance gain is not as high as in the previous cases. Note that in this scenario the acceleration is reduced compared to the previous scenarios, which explain the improved performance of the SBA estimator. This is consistent with the BER performance in Fig. 8(d), where the SBA estimator shows an improvement in the BER performance, though still being inferior to the CAF and MBA estimators.

Fig. 10 shows RMSE of estimation of the parameter a_2 by the MBA method in scenario 1 with the winter SSP. The RMSE is defined as

$$\text{RMSE} = \left[\frac{1}{N_{\text{MC}}}\sum_{i=1}^{N_{\text{MC}}}\left(a_2^{(i)} - \hat{a}_2^{(i)}\right)^2\right]^{1/2}, \tag{26}$$

where $a_2^{(i)}$ is the true value of the parameter a_2 in the ith trial and $\hat{a}_2^{(i)}$ is its estimate. In this scenario, the acceleration a is within the interval [-0.79, 0.79] m/s^2, i.e., a_2 is within an interval [-2.6, 2.6]$\times 10^{-4}$. It is seen that at SNR > 3 dB, the accuracy of the estimates is about 10% of the estimation interval. The RMSE performance in the other scenarios is close to that shown in Fig. 10.

VI. Sea trial

In this section, we compare the performance of the three Doppler estimation methods using data recorded in a deep-water sea trial, described as session F1-10 in [23]. In the sea trial, 376 guard-free OFDM symbols were transmitted at distances from 81 to 79 km. The transducer was towed at a depth of 200 m by a surface vessel moving at a speed of about 6–7 m/s towards a receiver. Due to the surface waves affecting the towing vessel, the transducer exhibited random oscillations around the main trajectory with an average period about 10 s [23]; this resulted in an (time-varying) acceleration between the transmitter and receiver. The receive omnidirectional hydrophone was slowly drifting at a depth of 400 m. Fig. 11 shows the SSP in the sea trial. The average SNR during the session is about 11 dB. Fig. 13 shows fluctuations of the channel impulse response in the sea trial, after removing the dominant time-varying delay corresponding to the transmitter speed 6 m/s. It is seen that the channel is characterized by a large number of fast-varying multipath components.

TABLE I
BER PERFORMANCE OF THE RECEIVER WITH THE THREE DOPPLER ESTIMATORS; DATA RATE: 1/2 BPS/HZ.

Doppler estimator	Code [3 7]	Code [23 35]	Code [561 753]
CAF	$4.5 \cdot 10^{-3}$	$8.5 \cdot 10^{-4}$	$2.0 \cdot 10^{-5}$
SBA	0.30	0.34	0.37
MBA	$4.8 \cdot 10^{-3}$	$9.2 \cdot 10^{-4}$	0

The BER performance is shown in Table I for different coding schemes, characterized by the code polynomial: [3 7], [23 35] or [561 753] in octal. It can be seen that for all the codes, the MBA method shows a performance similar to that of the CAF method, and it is significantly better than the performance provided by the SBA method. This result is similar to that obtained in Waymark numerical experiments in Section V.

To investigate the detection performance against SNR, we added extra noise recorded in the sea trial to the received signal. Fig. 14 shows the dependence of the BER on SNR for the code $[561\ 753]$. It can be seen that the MBA Doppler estimator provides the BER performance similar to that of the CAF method for the whole SNR range. At SNR = 11 dB, the MBA method provides the detection without errors.

The low performance of the SBA method can be explained using Fig. 12(a) and Fig. 12(b) showing $|A_{\text{MBA}}(\tau, \Omega_m)|$ with 7 Doppler sections, $m = 1, \ldots, 7$. The variable $m = 4$ corresponds to $\Omega_m = 0$, i.e., $A_{\text{MBA}}(\tau, \Omega_4) = A_{\text{SBA}}(\tau)$. Fig. 12(a) illustrates a case, when the peak of $|A_{\text{MBA}}(\tau, \Omega_m)|$ is in the Doppler section $m = 4$; in this case, the SBA method performs as the MBA method. However, in another case, illustrated by Fig. 12(b), the peak is at $m = 2$, the SBA method cannot detect the peak, and, consequently, the detection performance of the receiver is poor.

In this sea trial, the CAF method requires 61 Doppler sections, whereas the MBA method requires only 7 Doppler sections; thus, the complexity of the MBA method is significantly lower. However, the BER performance of the two methods is similar, whereas the SBA method cannot provide reliable detection.

VII. CONCLUSIONS

In this paper, we proposed and investigated a new multi-(branch) autocorrelation method for Doppler estimation in fast-varying UWA channels. The proposed method not only measures the time compression over the estimation interval, but also the gradient of the time compression, thus allowing more accurate (with time-varying sampling rate) resampling of the received signal to compensate for the Doppler distortions. The proposed method has been compared with a single-branch autocorrelation method and a method based on computing the cross-ambiguity function between the received and pilot signals. The results in shallow water simulation scenarios and in the deep sea trial demonstrate that the proposed method outperforms the single-branch autocorrelation method, and it is comparable in the performance to the method based on computation of the cross-ambiguity function. However, the proposed method requires significantly less computations.

APPENDIX A
DERIVATION OF MBA METHOD

We now show how the position of the maximum of $|\rho(\tau, \Omega, \mu)|$,

$$\{\tau_{\text{max}}, \Omega_{\text{max}}, \mu_{\text{max}}\} = \arg \max_{\tau, \Omega, \mu} |\rho(\tau, \Omega, \mu)|,$$

where $\rho(\tau, \Omega, \mu)$ is given by (10), relates to the Doppler parameters a_1 and a_2 in (9). Denote the product in the integral (10) as

$$z(t) = \widetilde{s}^*(t)\widetilde{s}(\mu t + \tau)e^{j\Omega t}. \tag{27}$$

Using (6), we obtain that

$$\begin{aligned} z(t) &= \widetilde{s}_0^*[t - \tau_d(t)]\widetilde{s}_0[(\mu t + \tau) - \tau_d(\mu t + \tau)] \\ &\times e^{j\omega_c[\tau_d(t) - \tau_d(\mu t + \tau)] + j\Omega t}. \end{aligned} \tag{28}$$

In order to achieve a maximum of $|\rho(\tau, \Omega, \mu)|$, according to the Cauchy-Bunyakovsky-Schwarz inequality [46], the following should be satisfied

$$\begin{aligned} & \widetilde{s}_0[t - \tau_d(t)]e^{-j\omega_c[\tau_d(t) - \tau_d(\mu t + \tau)] - j\Omega t} \\ = & \beta\widetilde{s}_0[(\mu t + \tau) - \tau_d(\mu t + \tau)], \end{aligned} \tag{29}$$

where β is an arbitrary constant independent of time. To satisfy this equality, we need, in particular, to guarantee that the exponent in (29) is independent of time t. With the approximation of the channel delay $\tau_d(t)$ as in (9), the component $\tau_d(t)-\tau_d(\mu t+\tau)$ in the exponent can be represented as

$$\begin{aligned} \tau_d(t)-\tau_d(\mu t+\tau) &= -(a_1\tau+a_2\tau^2) && (30)\\ &+ (a_1-a_1\mu-2a_2\mu\tau)t && (31)\\ &+ a_2(1-\mu^2)t^2. && (32)\end{aligned}$$

The first (time-independent) term (30) is absorbed in the constant β, and therefore it can be ignored. Below, we will show that the third term (32) can also be ignored. In order to remove the linear dependence of the exponent on time due to the term (31), the following should be satisfied:

$$\omega_c(a_1-a_1\mu-2a_2\mu\tau)+\Omega=0. \tag{33}$$

From this relationship, we arrive at the following estimate of the parameter a_2:

$$\hat{a}_2=\frac{\Omega_{\max}+a_1(1-\mu_{\max})\omega_c}{2\mu_{\max}\tau_{\max}\omega_c}, \tag{34}$$

where instead of a_1 its estimate can be substituted. Note that in many scenarios, $\mu_{\max}\approx 1$ and therefore the estimate in (34) can be simplified and made independent of a_1:

$$\hat{a}_2=\frac{\Omega_{\max}}{2\tau_{\max}\omega_c}. \tag{35}$$

To guarantee (29), we also need to equate arguments of $\widetilde{s}_0(\cdot)$ in both sides of this equation. Thus, we arrive at the relationship

$$t-\tau_d(t)=(\mu t+\tau)-\tau_d(\mu t+\tau)-T_s,$$

where we also take into account that the signal $\widetilde{s}_0(t)$ is periodic with the period T_s. Using (9), this condition takes the form

$$\begin{aligned} &(-a_1\tau-a_2\tau^2+\tau-T_s) && (36)\\ +\ &(a_1-a_1\mu-2a_2\mu\tau+\mu-1)t && (37)\\ +\ &a_2(1-\mu^2)t^2=0. && (38)\end{aligned}$$

Due to the time dependence present in this equation, we have to make all the three terms equal zero. Note that the last term (38) can be shown to be close to zero for all $t\in[-\Theta/2,\Theta/2]$ (see below), and therefore it can be ignored.

Making the first term (36) equal zero results in the following relationship:

$$\begin{aligned}\tau_{\max} &= \frac{1}{2a_2}\left(k-\sqrt{k^2-4a_2T_s}\right)\\ &\simeq \frac{T_s}{k}\left(1+\frac{a_2T_s}{k^2}\right),\end{aligned} \tag{39}$$

where $k=1-a_1$. This approximation is based on the facts that $k\simeq 1$, $a_2T_s\ll 1$ (see below), and the approximation $\sqrt{1-\varepsilon}\approx 1-\varepsilon/2-\varepsilon^2/8$, applicable if $|\varepsilon|\ll 1$. If $a_2=0$, we arrive at the estimate of the parameter a_1 given by

$$\hat{a}_1=1-\frac{T_s}{\tau_{\max}}, \tag{40}$$

which is exploited in the SBA estimator. For $a_2\neq 0$, from (39), after some algebra, we arrive at the following estimate of a_1:

$$\hat{a}_1=1-\frac{T_s}{\tau_{\max}}-\alpha\frac{\Omega_{\max}}{2\omega_c}, \tag{41}$$

where $\alpha=[T_s/(k\tau_{\max})]^2\simeq 1$.

Making the second term (37) equal zero results in the following relationship:

$$\mu_{\max}=\frac{1}{1-\frac{2a_2\tau_{\max}}{k}}, \tag{42}$$

where instead of a_2 its estimate $\hat{a}_2$ can be used. By substituting $\hat{a}_2$ from (34) into (42), we obtain

$$\mu_{\max}=1+\frac{\Omega_{\max}}{\omega_c}. \tag{43}$$

Thus, $\mu_{\max}$ can be found from $\Omega_{\max}$. This simplifies the Doppler estimation. According to (11), the statistic $|\rho(\tau,\Omega,\mu)|$ needs to be computed at a 3D grid. However, as $\mu_{\max}$ and $\Omega_{\max}$ are inter-dependent, only a 2D grid over (τ,Ω) is sufficient.

Previously, the term $a_2(1-\mu^2)t^2$ has been ignored for $t \in [-\Theta/2, \Theta/2]$ in (32) and (38); we now justify this step in our derivation. In many applications, it can be assumed that $a < 1$ m/s^2 [22], [29], [35]. Assuming also that Δ is the time-correlation interval of the signal $\widetilde{s}_0(t)$, which is given by $\Delta \approx 1/F$, the term $a_2 t^2(1-\mu^2)$ can be ignored if

$$\xi = |a_2 t^2 (1-\mu_{\text{max}}^2)| \ll \Delta \approx \frac{1}{F}.$$

From (42), taking into account that, for $|\varepsilon| \ll 1$, $(1-\varepsilon)^{-2} \simeq 1 + 2\varepsilon$ and $\tau_{\text{max}} \simeq T_s/k$, we approximately have

$$1 - \mu_{\text{max}}^2 \cong -\frac{4a_2 T_s}{k^2}.$$

Therefore, it is sufficient to require that

$$\xi_{\text{max}} = \max_{t \in [-\Theta/2, \Theta/2]} \xi = \frac{a^2 \Theta^2 T_s F}{4c^2} \ll 1.$$

In our experimental scenarios, we have $\Theta = 1$ s, $T_s = 1$ s, $F = 1024$ Hz, $c = 1500$ m/s, and $a < 1$ m/s^2. For all these scenarios, $\xi_{\text{max}} < 10^{-4} \ll 1$; thus, this requirement is satisfied with a significant margin.

When deriving (41), it was assumed that $a_2 T_s \ll 1$. Indeed, in our scenarios with $a < 1$ m/s^2, $a_2 T_s = aT_s/(2c) < 1/3000 \ll 1$, i.e., the assumption is satisfied with a significant margin.

We now analyze a possibility of setting $\mu = 1$ in (11) to further simplify the Doppler estimator. Such setting is possible if

$$|\Theta - \Theta\mu_{\text{max}}| < \Delta \approx \frac{1}{F},$$

or $\Theta F|1-\mu_{\text{max}}| < 1$, i.e., if the signal compression due to the factor μ_{max} over the observation interval Θ does not exceed the signal autocorrelation interval Δ. For our scenarios, from (42) we obtain

$$\Theta F|1-\mu_{\text{max}}| < 0.67 < 1,$$

i.e., this requirement is satisfied and we can set $\mu = 1$. Indeed, with higher values of the measurement interval Θ and the frequency bandwidth F, one of the components in (10) needs to be prescaled with a compression factor μ related to the frequency Ω as $\mu = 1 + \Omega/\omega_c$.

Appendix B
Complexity analysis

Below, we analyse the complexity of the CAF, MBA, and SBA methods in terms of real-valued multiply-accumulate (MAC) operations, which is the typical operation in DSP processors [47], [48].

A. CAF method

The computation of one Doppler section of the CAF requires the resampling, frequency correction, FFT, multiplication by the pilot sequence, IFFT, computation of (square) magnitudes, and finding a maximum (see Fig. 3). For the resampling, the linear interpolation is used, which requires 4 MACs for one complex-valued baseband sample. The frequency correction requires one complex-valued multiplication (4 MACs) per sample. The linear interpolation and frequency correction need to be done $N_s N_\tau$ times. The FFT and IFFT of size $N_s N_\tau$ are required. Assuming that the FFT/IFFT is implemented using the split-radix algorithm [49], its complexity is $P_{\text{FFT}} = 3N_s N_\tau \log_2(NN_\tau)$ MACs. For multiplication by the (real-valued) pilot sequence, $2N_s$ MACs are required. Instead of computing the CAF magnitude, it is more practical to compute its square magnitude, which requires $2N_s N_\tau$ MACs. Finding the magnitude maximum requires $N_s N_\tau$ MACs per Doppler section. In total, the computation of one Doppler section in the CAF Doppler estimator requires

$$P_{\text{CAF}} = 11N_s N_\tau + 2N_s + 6N_s N_\tau \log_2(N_s N_\tau) \text{ MACs}.$$

With $N_\tau = 2$ and $N_s = 1024$, the complexity is $P_{\text{CAF}} \approx 160 \cdot 10^3$ MACs. It can be seen that the complexity is dominated by computing the FFT and IFFT.

B. MBA and SBA methods

The computation of one Doppler section in the MBA method requires the frequency shift and computation of the autocorrelation according to (19), computation of (square) magnitudes, and finding the maximum. The frequency shift requires $4N_sN_\tau$ MACs. The further complexity will depend on the search area over the delay $\Lambda = [T_s - \tau_M, T_s + \tau_M]$. If the search area Λ is large, the autocorrelation is preferably computed using FFT and IFFT; on average (if FFTs in the consecutive estimation intervals are re-used), for such computation, one FFT and one IFFT are required. The autocorrelation computation requires $4N_sN_\tau + 2P_{\text{FFT}}$ MACs, where $4N_sN_\tau$ MACs are needed for multiplication of the FFT outputs. In total, when using FFTs for computation of the autocorrelation, the complexity of computing one Doppler section in the MBA method is given by

$$P_{\text{MBA}} = 8N_sN_\tau + 2P_{\text{FFT}} + 3|\Lambda| \text{ MACs},$$

where $|\Lambda|$ denotes the size (cardinality) of Λ and the last term is the complexity of computing the square magnitudes and finding the maximum; note that typically $|\Lambda| \ll N_sN_\tau$. In our scenarios, with a maximum speed of ± 7.3 m/s, we have $\tau_M \approx 4.9$ ms; thus, $|\Lambda| = 2\tau_M N_s N_\tau / T_s \approx 40$. With $N_\tau = 2$ and $N_s = 1024$, the complexity is $P_{\text{MBA}} \approx 152 \cdot 10^3$ MACs. It can be seen that similarly to the CAF computation, the MBA computation is dominated by the complexity of computing the FFT and IFFT, and therefore $P_{\text{MBA}} \approx P_{\text{CAF}}$.

However, if the search area Λ is small, the direct computation according to (19) could be less complicated. The direct computation of the autocorrelation requires $4|\Lambda|N_sN_\tau$ MACs. In this case, the total complexity is

$$P_{\text{MBA}} = 4N_sN_\tau + 4|\Lambda|N_sN_\tau + 3|\Lambda| \text{ MACs}.$$

With $N_\tau = 2$, $N_s = 1024$, and $|\Lambda| = 40$, the complexity is $P_{\text{MBA}} \approx 336 \cdot 10^3$ MACs, which is still higher than the complexity of the computation using FFTs. Thus, in our scenarios, the preferable implementation of the MBA method is the one based on FFTs and therefore the complexity of computation of one Doppler section P_{MBA} is almost the same as P_{CAF}.

The SBA method is a particular case of the MBA method, and its complexity P_{SBA} is similarly dominated by the computation of the FFT and IFFT. Therefore, we have $P_{\text{SBA}} \approx P_{\text{MBA}} \approx P_{\text{CFA}}$, and to compare the complexity of the Doppler estimators, it is enough to compare the number of Doppler sections $2N_d + 1$ required by the estimators. In the SBA method, $N_d = 0$, and only one Doppler section is used. For scenarios, considered in this paper, the value of N_d in the MBA method is significantly smaller than N_d in the CFA method. Thus, the complexity of the MBA method is significantly lower than the CAF complexity.

References

[1] Y. V. Zakharov and J. Li, "Autocorrelation method for estimation of Doppler parameters in fast-varying underwater acoustic channels," in *Underwater Acoustics, Conference and Exhibition, UACE-2015. Crete, Greece.*, 2015, pp. 1–4.

[2] B. S. Sharif, J. Neasham, O. R. Hinton, and A. E. Adams, "A computationally efficient Doppler compensation system for underwater acoustic communications," *IEEE Journal of Oceanic Engineering*, vol. 25, no. 1, pp. 52–61, 2000.

[3] B. Li, S. Zhou, M. Stojanovic, L. Freitag, and P. Willett, "Multicarrier communication over underwater acoustic channels with nonuniform Doppler shifts," *IEEE Journal of Oceanic Engineering*, vol. 33, no. 2, pp. 198–209, 2008.

[4] C. R. Berger, S. Zhou, J. C. Preisig, and P. Willett, "Sparse channel estimation for multicarrier underwater acoustic communication: From subspace methods to compressed sensing," *IEEE Transactions on Signal Processing*, vol. 58, no. 3, pp. 1708–1721, 2010.

[5] S. Yerramalli and U. Mitra, "Optimal resampling of OFDM signals for multiscale–multilag underwater acoustic channels," *IEEE Journal of Oceanic Engineering*, vol. 36, no. 1, pp. 126–138, 2011.

[6] G. Eynard and C. Laot, "Blind Doppler compensation scheme for single carrier digital underwater communications," in *IEEE OCEANS'2008*, pp. 1–5.

[7] M. Johnson, L. Freitag, and M. Stojanovic, "Improved Doppler tracking and correction for underwater acoustic communications," in *IEEE International Conference on Acoustics, Speech, and Signal Processing. ICASSP-97*, vol. 1, 1997, pp. 575–578.

[8] B. Li, S. Zhou, M. Stojanovic, L. Freitag, and P. Willett, "Non-uniform Doppler compensation for zero-padded OFDM over fast-varying underwater acoustic channels," in *IEEE OCEANS 2007-Europe*, pp. 1–6.

[9] M. Stojanovic and J. Preisig, "Underwater acoustic communication channels: Propagation models and statistical characterization," *IEEE Communications Magazine*, vol. 47, no. 1, pp. 84–89, 2009.

[10] C. Liu, Y. V. Zakharov, and T. Chen, "Doubly selective underwater acoustic channel model for a moving transmitter/receiver," *IEEE Transactions on Vehicular Technology*, vol. 61, no. 3, pp. 938–950, 2012.

[11] J. S. Dhanoa and R. F. Ormondroyd, "Combined differential Doppler and time delay compensation for an underwater acoustic communication system," in *MTS/IEEE OCEANS'2002*, vol. 1, pp. 581–587.

[12] S. F. Mason, C. R. Berger, S. Zhou, and P. Willett, "Detection, synchronization, and Doppler scale estimation with multicarrier waveforms in underwater acoustic communication," *IEEE Journal on Selected Areas in Communications*, vol. 26, no. 9, pp. 1638–1649, 2008.

[13] A. Y. Kibangou, C. Siclet, and L. Ros, "Joint channel and Doppler estimation for multicarrier underwater communications," in *ICASSP*, 2010, pp. 5630–5633.

[14] X. Xu, Z. Wang, S. Zhou, and L. Wan, "Parameterizing both path amplitude and delay variations of underwater acoustic channels for block decoding of orthogonal frequency division multiplexing," *The Journal of the Acoustical Society of America*, vol. 131, no. 6, pp. 4672–4679, 2012.

[15] Z. Wang, S. Zhou, J. C. Preisig, K. R. Pattipati, and P. Willett, "Clustered adaptation for estimation of time-varying underwater acoustic channels," *IEEE Transactions on Signal Processing*, vol. 60, no. 6, pp. 3079–3091, 2012.

[16] N. Santos, A. Matos, and N. Cruz, "Navigation of an autonomous underwater vehicle in a mobile network," *IEEE OCEANS 2008*, vol. 1-4, pp. 1–5, 15-18 Sept. 2008.

[17] R. N. Smith, Y. Chao, B. H. Jones, D. A. Caron, P. P. Li, and G. S. Sukhatme, "Trajectory design for autonomous underwater vehicles based on ocean model predictions for feature tracking," in *Field and Service Robotics*. Springer, 2010, pp. 263–273.

[18] B. He, H. Zhang, C. Li, S. Zhang, Y. Liang, and T. Yan, "Autonomous navigation for autonomous underwater vehicles based on information filters and active sensing," *Sensors*, vol. 11, no. 11, pp. 10 958–10 980, 2011.

[19] F. García C., A. Guerrero G. *et al.*, "Intelligent navigation for a solar powered unmanned underwater vehicle," *International Journal of Advanced Robotic Systems*, vol. 10, no. 185, 2013.

[20] O. Gal, "Unified trajectory planning algorithms for autonomous underwater vehicle navigation," *ISRN Robotics*, vol. 2013, 2013.

[21] J. McColgan and E. W. McGookin, "Coordination of multiple biomimetic autonomous underwater vehicles using strategies based on the schooling behaviour of fish," *Robotics*, vol. 5, no. 1, p. 2, 2016.

[22] N. Parrish, S. Roy, and P. Arabshahi, "Symbol by symbol Doppler rate estimation for highly mobile underwater OFDM," in *Proceedings of the Fourth ACM International Workshop on UnderWater Networks, Berkeley, CA, USA*. ACM, Nov. 2009, pp. 1–8.

[23] Y. V. Zakharov and A. K. Morozov, "OFDM transmission without guard interval in fast-varying underwater acoustic channels," *IEEE Journal of Oceanic Engineering*, vol. 40, no. 1, pp. 144–158, 2015.

[24] T. Yang, "Underwater telemetry method using Doppler compensation," Jan. 28 2003, US Patent 6,512,720.

[25] L. Wan, Z. Wang, S. Zhou, T. C. Yang, and Z. Shi, "Performance comparison of Doppler scale estimation methods for underwater acoustic OFDM," *Journal of Electrical and Computer Engineering*, vol. 2012, pp. 1–11, 2012.

[26] M. Stojanovic, J. A. Catipovic, and J. G. Proakis, "Phase-coherent digital communications for underwater acoustic channels," *IEEE Journal of Oceanic Engineering*, vol. 19, no. 1, pp. 100–111, 1994.

[27] T. J. Riedl and A. C. Singer, "Broadband Doppler compensation: Principles and new results," in *Conference Record of the Forty Fifth Asilomar Conference on Signals, Systems and Computers (ASILOMAR)*, 2011, pp. 944–946.

[28] K. A. Perrine, K. F. Nieman, T. L. Henderson, K. H. Lent, T. J. Brudner, and B. L. Evans, "Doppler estimation and correction for shallow underwater acoustic communications," in *2010 IEEE Conference Record of the Forty Fourth Asilomar Conference on Signals, Systems and Computers*, pp. 746–750.

[29] T. Arikan, T. Riedl, A. Singer, and J. Younce, "Comparison of OFDM and single-carrier schemes for Doppler tolerant acoustic communications," in *IEEE OCEANS-2015, Genova*, 2015, pp. 1–7.

[30] Y. V. Zakharov and V. P. Kodanev, "Experimental study of an underwater acoustic communication system with pseudonoise signals," *Journal of Acoustical Physics*, vol. 40, no. 9, pp. 707–715, 1994.

[31] Y. V. Zakharov and V. P. Kodanev, "Doppler scattering adaptive reception in a hydroacoustic communication channel," *Journal of Acoustical Physics*, vol. 41, no. 2, pp. 219–223, 1995.

[32] G. Jourdain, "Characterization of the Underwater Channel Application to Communication," in *Issues in Acoustic Signal-Image Processing and Recognition*. Springer, 1983, pp. 197–209.

[33] S. M. Kay and S. B. Doyle, "Rapid estimation of the range-Doppler scattering function," *IEEE Transactions on Signal Processing*, vol. 51, no. 1, pp. 255–268, 2003.

[34] A. E. Abdelkareem, B. S. Sharif, C. C. Tsimenidis, J. A. Neasham, and O. R. Hinton, "Low-complexity Doppler compensation for OFDM-based underwater acoustic communication systems," in *IEEE OCEANS-2011, Spain*, 2011, pp. 1–6.

[35] A. E. Abdelkareem, B. S. Sharif, and C. C. Tsimenidis, "Adaptive time varying Doppler shift compensation algorithm for OFDM-based underwater acoustic communication systems," *Ad Hoc Networks*, vol. 45, pp. 104–119, 2016.

[36] J. C. Peterson and M. B. Porter, "Ray/beam tracing for modeling the effects of ocean and platform dynamics," *IEEE Journal of Oceanic Engineering*, vol. 38, no. 4, pp. 655–665, 2013.

[37] P. Qarabaqi and M. Stojanovic, "Statistical characterization and computationally efficient modeling of a class of underwater acoustic communication channels," *IEEE Journal of Oceanic Engineering*, vol. 38, no. 4, pp. 701–717, 2013.

[38] M. B. Porter, "The BELLHOP Manual and Users Guide: Preliminary draft," *Heat, Light, and Sound Research, Inc., La Jolla, CA, USA, Tech. Rep*, 2011.

[39] B. Henson, J. Li, Y. V. Zakharov, and C. Liu, "Waymark baseband underwater acoustic propagation model," in *Underwater Communications and Networking (UComms)*, 2014, pp. 1–5.

[40] B. Henson, "Waymark based underwater acoustic channel model," Apr. 29 2017, https://www.york.ac.uk/electronic-engineering/research/communication-technologies/underwater-networks/resources/.

[41] Y. V. Zakharov and A. K. Morozov, "Adaptive sparse channel estimation for guard-free OFDM transmission in underwater acoustic channels," *Proceedings of UAC-2013*, June 2013.

[42] J. G. Proakis, "Digital communications," *McGraw Hill, New York*, 1995.

[43] W. W. S. Wei, *Time series analysis*. Addison-Wesley publ Reading, 1994.

[44] R. M. Hamson and R. M. Heitmeyer, "Environmental and system effects on source localization in shallow water by the matched-field processing of a vertical array," *The Journal of the Acoustical Society of America*, vol. 86, no. 5, pp. 1950–1959, 1989.

[45] D. F. Gingras, "Robust broadband matched-field processing: performance in shallow water," *IEEE Journal of Oceanic Engineering*, vol. 18, no. 3, pp. 253–264, 1993.

[46] I. S. Gradshteyn and I. M. Ryzhik, *Table of integrals, series, and products*. Academic Press, Inc., San Diego, CA, 2000.

[47] L. J. Karam, I. A. Kamal, A. Gatherer, G. Frantz, D. V. Anderson, B. L. Evans *et al.*, "Trends in multicore DSP platforms," *IEEE Signal Processing Magazine*, vol. 26, no. 6, pp. 38–49, 2009.

[48] A. Bateman and S. I. Paterson, *The DSP handbook*. Prentice-Hall, 2002.

[49] P. Duhamel and H. Hollmann, "Split-radix FFT algorithm," *Electronics letters*, vol. 20, no. 1, pp. 14–16, 1984.

Jianghui Li received the B.S. degree in communications engineering from Huazhong University of Science and Technology, Wuhan, China in 2011, the M.Sc. degree in communications engineering, and the Ph.D. degree with receiving the K. M. Stott Prize for excellent research in electronics engineering from the University of York, U.K., in 2013 and 2017, respectively.

From 2011 to 2012, he served as a Research Assistant with the Chinese Academy of Sciences, Beijing, China. Since 2017, he has been a Research Fellow with the University of Southampton and National Oceanography Centre, U.K.. His current research interests include adaptive signal processing, underwater acoustics, and wireless communications.

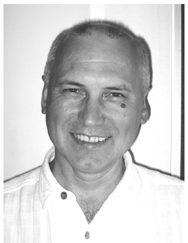

Yuriy V. Zakharov received the M.Sc. and Ph.D. degrees in electrical engineering from the Power Engineering Institute, Moscow, Russia, in 1977 and 1983, respectively.
From 1977 to 1983, he was with the Special Design Agency in the Moscow Power Engineering Institute. From 1983 to 1999, he was with the N. N. Andreev Acoustics Institute, Moscow. From 1994 to 1999, he was with Nortel as a DSP Group Leader. Since 1999, he has been with the Communications Research Group, University of York, U.K., where he is currently a Reader in the Department of Electronics. His research interests include signal processing, communications, and acoustics.

Benjamin Henson Benjamin Henson received his M.Eng. degree in Electronic Engineering in 2001 from University of York, U.K.. From 2002 to 2008, he worked as an engineer for Snell & Wilcox Ltd. designing broadcast equipment. From 2008 to 2009, he worked for SRD Ltd. on image sonar designs. He received an M.Sc degree in Natural Computation in 2011 from University of York, U.K.. Then, from 2011 to 2013, he worked on laser measurement equipment for Renishaw plc. He is currently working towards the Ph.D. degree in Electronic Engineering in the Communications Research Group with the Department of Electronics at University of York. His interests include signal and image processing, acoustics.

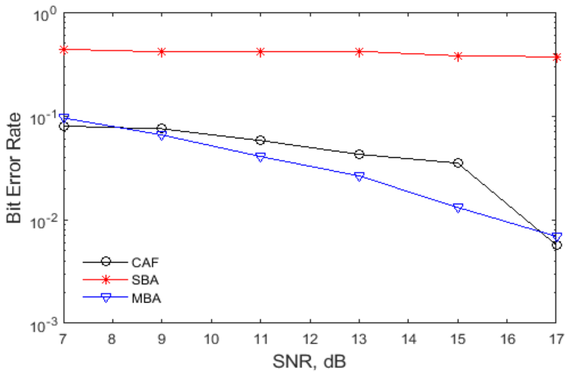

(a) Summer SSP, transmitter moves towards receiver, 10 km, 1/2 bps/Hz.

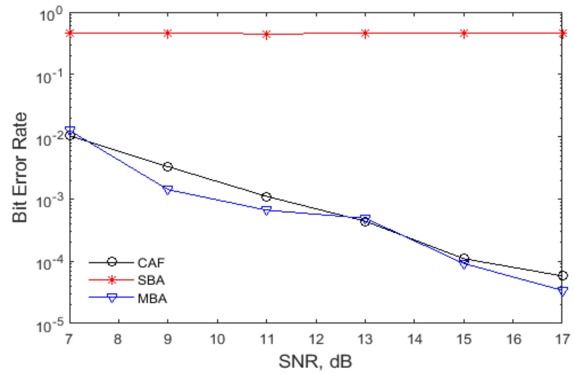

(b) Winter SSP, transmitter moves towards receiver, 20 km, 1/2 bps/Hz.

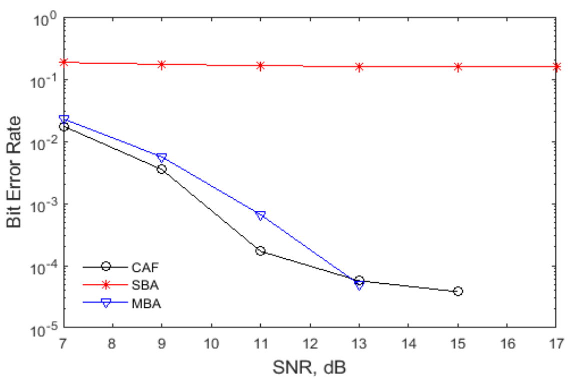

(c) Summer SSP, transmitter moves past receiver, 2 km, 1/3 bps/Hz.

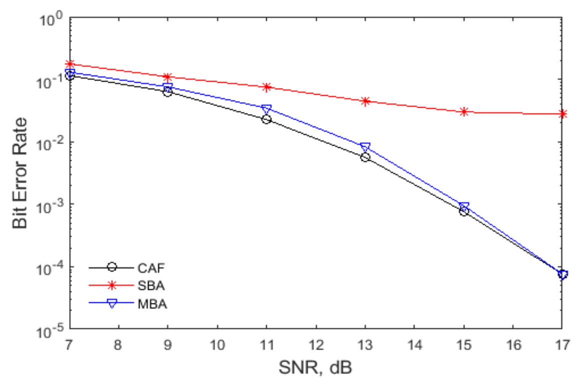

(d) Summer SSP, flower circle movement, 5 km, 1/3 bps/Hz.

Fig. 8. BER performance of the receiver with the three Doppler estimation methods in the four simulation scenarios (environment, scenario, distance, data rate).

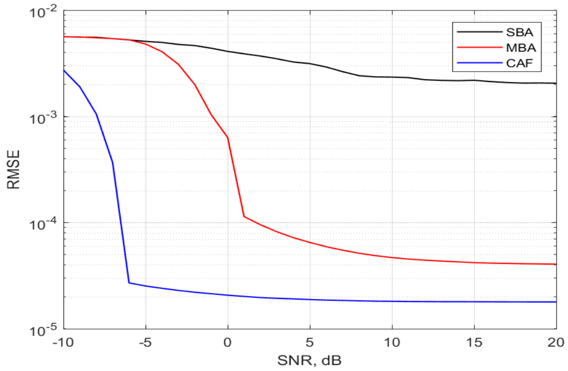

(a) Summer SSP, transmitter moves towards receiver, 10 km, 1/2 bps/Hz.

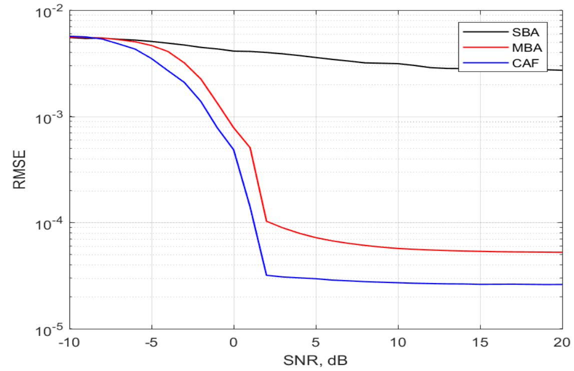

(b) Winter SSP, transmitter moves towards receiver, 20 km, 1/2 bps/Hz.

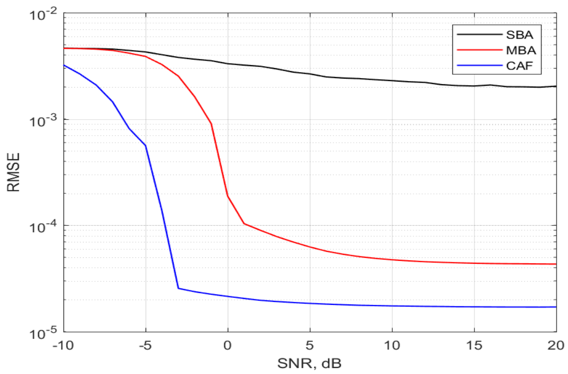

(c) Summer SSP, transmitter moves past receiver, 2 km, 1/3 bps/Hz.

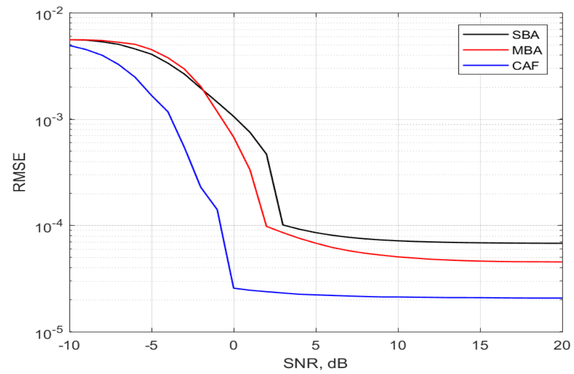

(d) Summer SSP, flower circle movement, 5 km, 1/3 bps/Hz.

Fig. 9. RMSE performance of estimating the parameter a_1 by the three Doppler estimation methods in four 'synthetic' scenarios, corresponding to the scenarios in Fig. 7 and Fig. 8 (environment, scenario, distance, data rate).

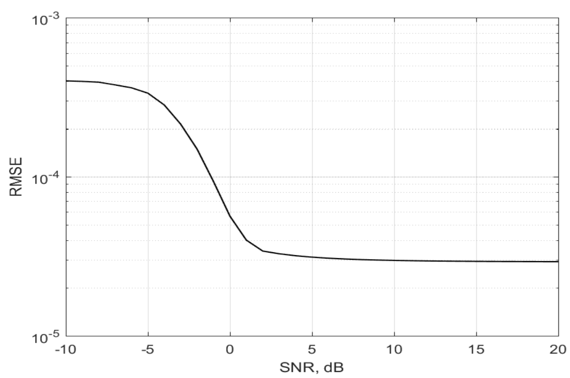

Fig. 10. RMSE performance of estimating the parameter a_2 by the MBA method using (14).

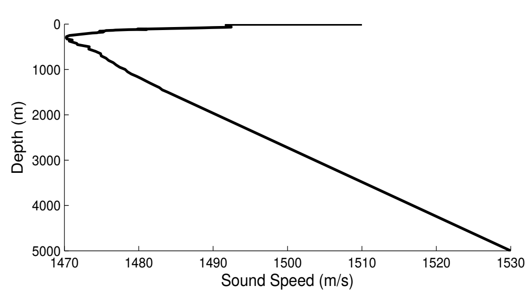

Fig. 11. SSP in the sea trial.

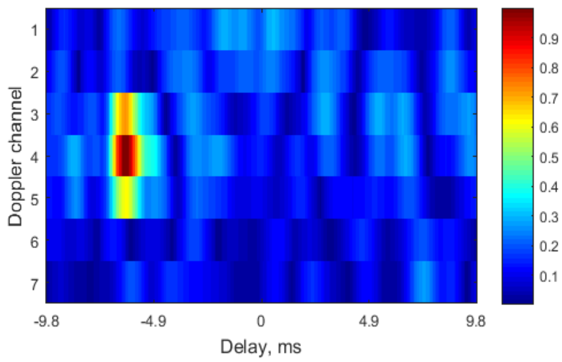

(a) A case of low acceleration.

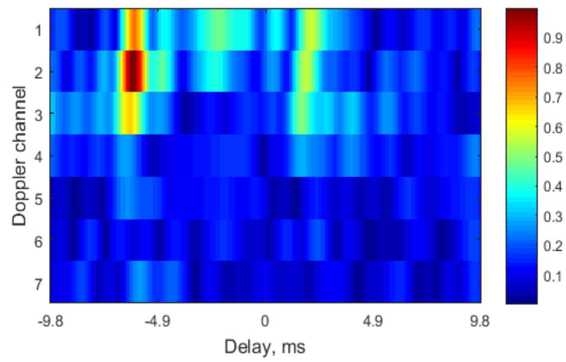

(b) A case of high acceleration.

Fig. 12. Examples of the time-frequency autocorrelation function $|A_{\text{MBA}}(\tau, \Omega_m)|$ in the sea trial. The delay values are shown with respect to the delay $T_s = 1$ s.

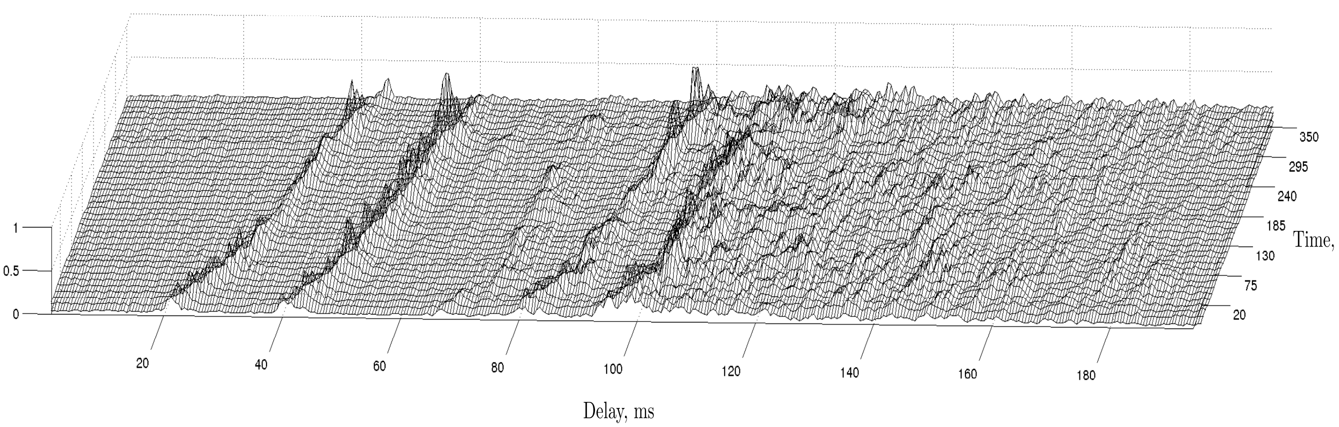

Fig. 13. Fluctuations of the channel impulse response in the sea trial.

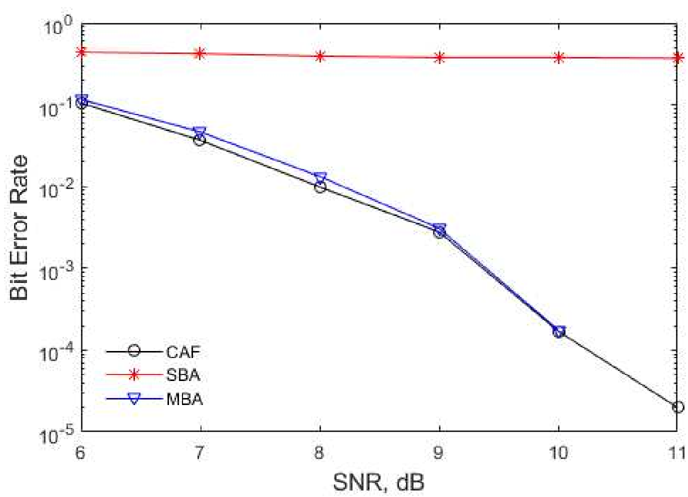

Fig. 14. BER performance of the receiver with the three Doppler estimators in the sea experiment; data rate 1/2 bps/Hz.